

Cosmological constraints on scalar-tensor gravity and the variation of the gravitational constant

Junpei Ooba¹, Kiyotomo Ichiki^{1,2}, Takeshi Chiba³, and Naoshi Sugiyama^{1,2,4}

¹*Department of physics and astrophysics, Nagoya University, Nagoya 464-8602, Japan*

²*Kobayashi-Maskawa Institute for the Origin of Particles and the Universe, Nagoya University, Nagoya 464-8602, Japan*

³*Department of Physics, College of Humanities and Sciences, Nihon University, Tokyo 156-8550, Japan*

⁴*Kavli Institute for the Physics and Mathematics of the Universe (Kavli IPMU), The University of Tokyo, Chiba 277-8582, Japan*

.....
Cosmological constraints on the scalar-tensor theory of gravity by analyzing the angular power spectrum data of the cosmic microwave background (CMB) obtained from the Planck 2015 results together with the baryon acoustic oscillations (BAO) data are presented. We find that the inclusion of the BAO data improves the constraints on the time variation of the effective gravitational constant by more than 10%, that is, the time variation of the effective gravitational constant between the recombination and the present epochs is constrained as $G_{\text{rec}}/G_0 - 1 < 1.9 \times 10^{-3}$ (95.45%C.L.) and $G_{\text{rec}}/G_0 - 1 < 5.5 \times 10^{-3}$ (99.99%C.L.). We also discuss the dependence of the constraints on the choice of the prior.
.....

Subject Index E03, E50, E60, E63

1. Introduction

The existence of scalar fields whose vacuum expectation values determine the physical constants is generically predicted by the recent attempts toward unifying all elementary forces in nature based on string theory [1]. In this context, scalar-tensor theories of gravity are natural alternative to the Einstein gravity since they arise from the low-energy limit of string theory. In the scalar-tensor theories of gravity, a scalar field couples to the Ricci scalar, which provides a natural framework for realizing the time variation of the gravitational constant via the dynamics of the scalar field. In the Jordan-Brans-Dicke theory of gravity [2], which is the simplest example of scalar-tensor theories, a constant coupling parameter ω is introduced. In more general scalar-tensor theories [3], ω is promoted to a function of the Brans-Dicke scalar field ϕ . In the limit $\omega \rightarrow \infty$, the Einstein gravity is recovered and the gravitational constant becomes a constant in time.

The coupling parameter ω has been constrained by several solar system experiments. For instance, the weak-field experiment conducted in the Solar System by the Cassini mission

has put strong constraints on the post-Newtonian deviation from the Einstein gravity, where ω is constrained as $\omega > 43000$ at 2σ level [4, 5].

On cosmological scales, the possibility of constraining the Brans-Dicke theory by temperature and polarization anisotropies of the cosmic microwave background (CMB) was suggested in [6], and Nagata *et al.* [7] first placed constraints on a general scalar-tensor theory called the harmonic attractor model including the Jordan-Brans-Dicke theory [8]. In this model the scalar field has a quadratic effective potential of positive curvature in the Einstein frame, and the Einstein gravity is an attractor that naturally suppresses any deviations from the Einstein gravity in the present epoch. Nagata *et al.* reported that the present-day value of ω is constrained as $\omega > 1000$ at 2σ level by analyzing the CMB data from the Wilkinson Microwave Anisotropy Probe (WMAP). Moreover, the gravitational constant at the recombination epoch G_{rec} relative to the present gravitational constant G_0 is constrained as $G_{\text{rec}}/G_0 < 1.05$ (2σ). These constraints basically come from the fact that the size of the sound horizon at the recombination epoch, which determines the characteristic angular scale in the angular power spectrum of CMB anisotropies, depends on the amounts of matter and baryon contents and on the strength of gravity at that epoch. Recently, we have analyzed the CMB power spectra data from Planck 2015 [9] in the harmonic attractor model to put constraints on the deviations from the general relativity [10]. We find an order-of-magnitude improvement on the change of G : $G_{\text{rec}}/G_0 < 1.0056$ (1.0115) at 95.45% C.L. (99.99% C.L.) [10].

Acoustic peaks in the CMB power spectrum are transferred to peaks in baryons through the coupling between photons and baryons through the Thomson scattering, and these acoustic peaks are later imprinted on the matter power spectrum which are known as baryon acoustic oscillations (BAO). BAO have been measured by a number of galaxy redshift surveys. Since the BAO measurements are basically geometrical like CMB acoustic peaks, they can be used to break parameter degeneracies in the analysis based solely on the CMB data. In this paper, we further improve the constraints on the scalar-tensor theory by including the recent measurements of BAO [11–13].

The remainder of the paper is organized as follows. In Sec. 2 we explain the scalar-tensor cosmological model and describes our method for constraining the scalar-tensor coupling parameters in Sec. 3. In Sec. 4, we compare the model with the CMB data and BAO data. The prior dependence of the analysis is also discussed. We summarize our results in Sec. 5.

2. Model

The action describing a general massless scalar-tensor theory in the Jordan frame is given by [14]

$$S = \frac{1}{16\pi G_0} \int d^4x \sqrt{-g} \left[\phi R - \frac{\omega(\phi)}{\phi} (\nabla\phi)^2 \right] + S_{\text{m}}[\psi, g_{\mu\nu}], \quad (1)$$

where G_0 is the present-day Newtonian gravitational constant, $S_{\text{m}}[\psi, g_{\mu\nu}]$ is the matter action which is a function of the matter variable ψ and the metric $g_{\mu\nu}$. We regard this “Jordan frame metric” defines the lengths and times actually measured by laboratory rods and clocks since in the action Eq.(1) matter is universally coupled to $g_{\mu\nu}$ [15, 16]. The function $\omega(\phi)$ is the dimensionless coupling parameter which depends on the scalar field ϕ . The deviation from the Einstein gravity depends on the asymptotic value of ϕ at spatial infinity. According to the cosmological attractor scenario [8], the dynamics of ϕ in the Friedmann universe

is analogous to that of a particle attracted toward the minimum of its effective potential with a friction (the Hubble friction in the Friedmann universe) in the Einstein frame. The effective potential corresponds to the logarithm of the conformal factor. Since a potential near a minimum is generically parabolic, we study the case where the effective potential is quadratic. This setup corresponds to $\omega(\phi)$ of the following form,

$$2\omega(\phi) + 3 = \{\alpha_0^2 - \beta \ln(\phi/\phi_0)\}^{-1}, \quad (2)$$

where ϕ_0 is the present value of ϕ and α_0 and β are model parameters. See Appendix A for details.

The background equations for a Friedmann universe are

$$\rho' = -3\frac{a'}{a}(\rho + p), \quad (3)$$

$$\left(\frac{a'}{a}\right)^2 + K = \frac{8\pi G_0 \rho a^2}{3\phi} - \frac{a' \phi'}{a \phi} + \frac{\omega}{6} \left(\frac{\phi'}{\phi}\right)^2, \quad (4)$$

$$\phi'' + 2\frac{a'}{a}\phi' = \frac{1}{2\omega + 3} \left\{ 8\pi G_0 a^2(\rho - 3p) - \phi'^2 \frac{d\omega}{d\phi} \right\}, \quad (5)$$

where a is the cosmological scale factor and the prime notation denotes a derivative with respect to the conformal time, ρ and p are the total energy density and pressure, respectively, and K denotes a constant spatial curvature.

The effective gravitational constant measured by Cavendish-type experiments is given by [15]

$$G(\phi) = \frac{G_0}{\phi} \frac{2\omega(\phi) + 4}{2\omega(\phi) + 3}. \quad (6)$$

The present value of ϕ must yield the present-day Newtonian gravitational constant and satisfy the expression of $G(\phi_0) = G_0$. Thus, we have

$$\phi_0 = \frac{2\omega_0 + 4}{2\omega_0 + 3} = 1 + \alpha_0^2, \quad (7)$$

where ω_0 is the present value of $\omega(\phi)$.

Typical evolutions of ϕ and $G(\phi)$ are shown in Figs. 1 and 2, respectively. Here $h = 0.68$, $\Omega_m h^2 = 0.14$ are assumed where h is the dimensionless Hubble parameter and Ω_m is the matter density parameter. In the radiation-dominated epoch, ϕ becomes almost constant because the pressure of the relativistic component in Eq. (5) is $p = \rho/3$. After the matter-radiation equality, ϕ begins to increase up to the present value ϕ_0 . The variation in the value of ϕ alters the Hubble parameter in the early universe from its value under the Einstein gravity through Eq. (4). Therefore, we expect that the observational data during the matter dominated era, such as CMB and especially BAO, are useful in putting constraints on the scalar-tensor gravity.

The typical CMB temperature anisotropy spectra are shown in Fig. 3. Here $h = 0.6782$, $\Omega_b h^2 = 0.02227$, $\Omega_c h^2 = 0.1185$, $\tau_{\text{reio}} = 0.067$, $\ln(10^{10} A_s) = 3.064$, $n_s = 0.9684$, $T_{\text{CMB}} = 2.7255$ K, $N_{\text{eff}} = 3.046$ are assumed for the parameters of the Λ CDM model where Ω_b and Ω_c are the density parameters for baryon and cold dark matter components, respectively, τ_{re} is the reionization optical depth, and A_s and n_s are the amplitude and spectral index of primordial curvature fluctuations, respectively. Since the locations of the acoustic peaks

and the damping scale depend differently on the horizon length at recombination, we can constrain the ϕ -induced variations in the horizon scale by analyzing the measurements of the CMB anisotropies at small angular scales. The positions of the acoustic peaks are proportional to the horizon length ($\propto H^{-1}$), while that of the damping scale is less affected by it ($\propto \sqrt{H^{-1}}$). Therefore, the locations of the first peak and the diffusion tail in the angular power spectrum become closer as the expansion rate becomes larger, suppressing the small scale peaks, as shown in Fig. 3.

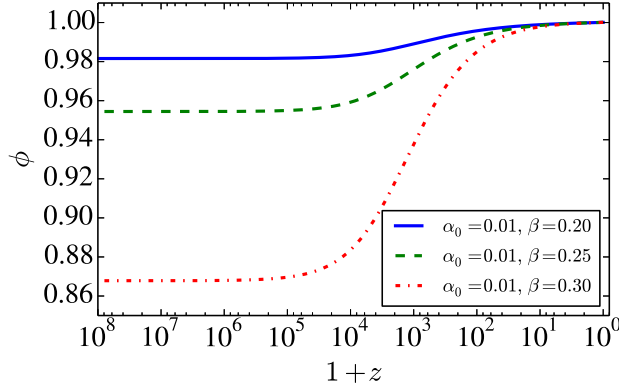


Fig. 1 Time evolution of ϕ in the scalar-tensor Λ CDM model, with the parameters as indicated in the figure. The other cosmological parameters are fixed to the standard values.

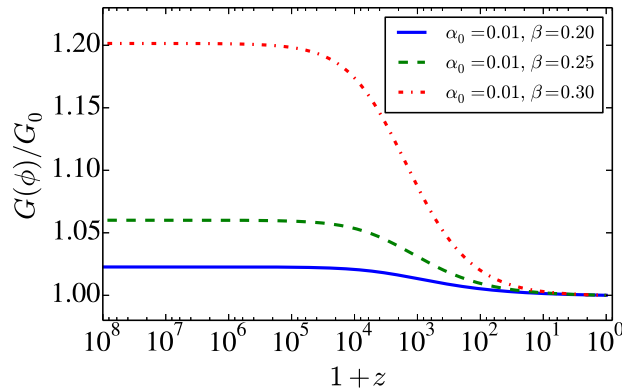


Fig. 2 Time evolution of $G(\phi)/G_0$ in the scalar-tensor models with the same parameters as in Fig. 1. The effective gravitational constant $G(\phi)$ is inversely proportional to the scalar field ϕ through Eq. (6).

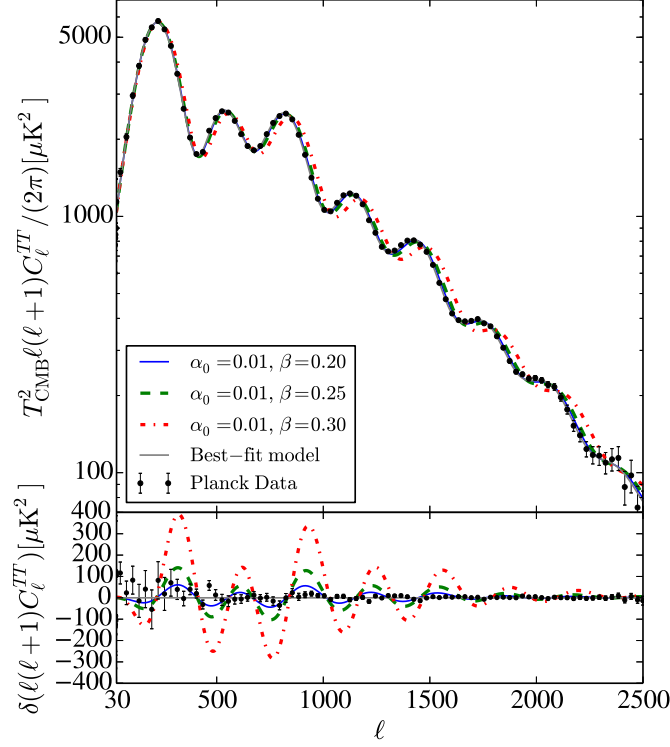


Fig. 3 CMB temperature anisotropy spectra in the scalar-tensor models with the Λ CDM parameters. The data points with error bars represent the Planck data. The gray solid line shows the best-fit Λ CDM theoretical model fitted to the Planck + BAO data. Residuals with respect to the best-fit model are shown in the lower panel.

3. METHODS

To compute the temperature and polarization fluctuations in the CMB and the lensing potential power spectra, we numerically solve the equations in the model described in the previous section modifying the publicly available numerical code, CLASS [17]. The data are analyzed using the Markov Chain Monte Carlo (MCMC) method with Monte Python [18] developed in the CLASS code. In our calculations, we consider (α_0, β) in Eq. (2), which characterize the scalar-tensor theory, in addition to the parameters of the Λ CDM model.

We set the priors for the standard cosmological parameters as

$$\begin{aligned}
 H_0 &\in (30, 100), \quad \Omega_b h^2 \in (0.005, 0.04), \\
 \Omega_c h^2 &\in (0.01, 0.5), \quad \tau_{\text{reio}} \in (0.005, 0.5), \\
 \ln(10^{10} A_s) &\in (0.5, 10), \quad n_s \in (0.5, 1.5),
 \end{aligned}
 \tag{8}$$

and for α_0 and β as

$$\log_{10}(\alpha_0) \in (-6, -0.5),
 \tag{9}$$

$$\beta \in (0, 0.4).
 \tag{10}$$

The CMB temperature and the effective number of neutrinos were set to $T_{\text{CMB}} = 2.7255$ K from COBE [19] and $N_{\text{eff}} = 3.046$, respectively. The primordial helium fraction Y_{He} is inferred from the standard Big Bang nucleosynthesis, as a function of the baryon density.

We compare our results with the CMB angular power spectrum data from the Planck 2015 mission [9] and the measurements of the baryon acoustic oscillations (BAO) in the matter power spectra obtained by 6dF Galaxy Survey (6dFGS) [11], Baryon Oscillation Spectroscopic Survey (BOSS) (LOWZ and CMASS) [12] and Sloan Digital Sky Survey (SDSS) main galaxy sample (MGS) [13]. The Planck data include the auto power spectra of temperature and polarization anisotropies (TT and EE), their cross-power spectrum (TE), and the lensing potential power spectrum. The data of the BAO measurements are the values of D_V/r_{drag} as shown in Fig. 4, where r_{drag} is the coming sound horizon at the end of the baryon drag epoch and D_V is the function of the angular diameter distance $D_A(z)$ and Hubble parameter $H(z)$ defined by

$$D_V(z) = \left[(1+z)^2 D_A^2(z) \frac{z}{H(z)} \right]^{1/3}. \quad (11)$$

The BAO can be used to constrain the scalar-tensor cosmological models as the CMB: the length of the sound horizon at the end of the baryon drag epoch scales as $r_{\text{drag}} \propto H^{-1}(z_{\text{drag}}) \propto G_{\text{drag}}^{-1}$ while the geometric distance indicator scales as $D_V \propto H^{-1} \propto G_{\text{bao}}^{-1}$, where G_{drag} and G_{bao} are the gravitational constant at the redshifts of the baryon drag epoch and the BAO measurements, respectively. Therefore, if $G_{\text{drag}} \neq G_{\text{bao}}$, the BAO data can be used to constrain the scalar-tensor cosmological models. Indeed, the models considered in this paper always predict $G_{\text{drag}} > G_{\text{bao}}$ leading to a larger D_V/r_{drag} , as is shown in Fig. 4.

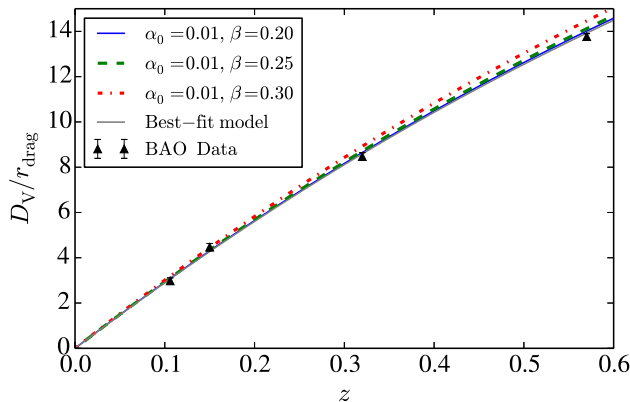


Fig. 4 Time evolutions of D_V/r_{drag} in the scalar-tensor models with the same parameters as in Fig. 1. The data points with error bars represent the data of the BAO measurements. The gray solid line shows the best-fit Λ CDM theoretical model fitted to the Planck + BAO data.

The two point correlation function is defined by

$$\xi(r) = \int \frac{k^2 dk}{2\pi^2} \frac{\sin(kr)}{kr} P(k), \quad (12)$$

where r is the distance, k is the wave number, $P(k)$ is the power spectrum of primordial curvature fluctuations. Some typical examples in the scalar-tensor model are shown in Fig. 5. The BAO peak scale is proportional to r_{drag} , and therefore, the location of the BAO peak moves to smaller scale as the G_{drag} becomes larger.

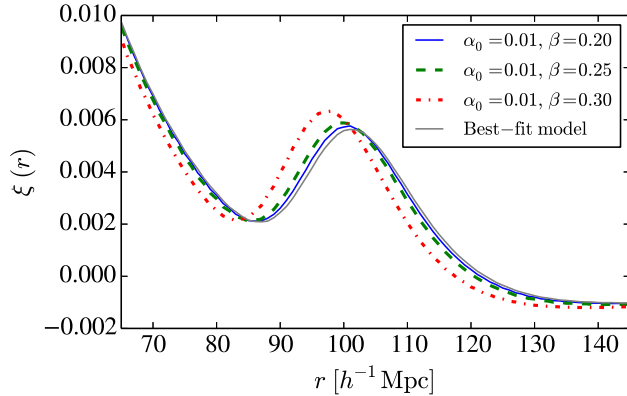


Fig. 5 Two point correlation function $\xi(r)$ in the scalar-tensor models with the same parameters as in Fig. 1. The gray solid line shows the best-fit Λ CDM theoretical model fitted to the Planck + BAO data.

Because the variation of the gravitational constant could alter the distance to the last scattering surface of the CMB through the change in the Hubble parameter, its effect on the angular power spectrum may degenerate with the effects of spatial curvature in the Friedmann universe and effective number of relativistic degree of freedom. Therefore, we separately perform MCMC analyses for models with the spatial curvature (Ω_K) and with the effective number of relativistic degree of freedom (N_{eff}). We set the priors for Ω_K and N_{eff} as

$$\Omega_K \in (-0.5, 0.5), \quad (13)$$

$$N_{\text{eff}} \in (1, 5), \quad (14)$$

while the same priors are used for the other standard cosmological parameters and (α_0, β) as shown in Eqs. (8), (9) and (10).

4. RESULTS

We show the results of the parameter constraints for flat universe models (Sec. 4.1), for non flat universe models (Sec. 4.2) and for models with N_{eff} (Sec. 4.3).

4.1. Flat universe case

In Fig. 6, we show the constraint contours in the $\log_{10}(\alpha_0^2) - \beta$ plane, where the other parameters are marginalized. We find that the constraints on $\log_{10}(\alpha_0^2)$ and β are

approximately given by

$$\log_{10}(\alpha_0^2) < -3.9 - 20\beta^2 \quad (95.45\%), \quad (15)$$

$$\log_{10}(\alpha_0^2) < -2.8 - 20\beta^2 \quad (99.99\%), \quad (16)$$

where the number in the parenthesis denotes the confidence level (C.L.). These results can be translated into the present-day value of the coupling parameter ω at $\beta = 0$ using Eq. (2) as

$$\omega > 3254 \quad (95.45\%), \quad (17)$$

$$\omega > 307 \quad (99.99\%). \quad (18)$$

These limits are little changed compared with those obtained by the Planck data alone: $\omega > 3224$ (303) at 95.45% C.L. (99.99% C.L.).

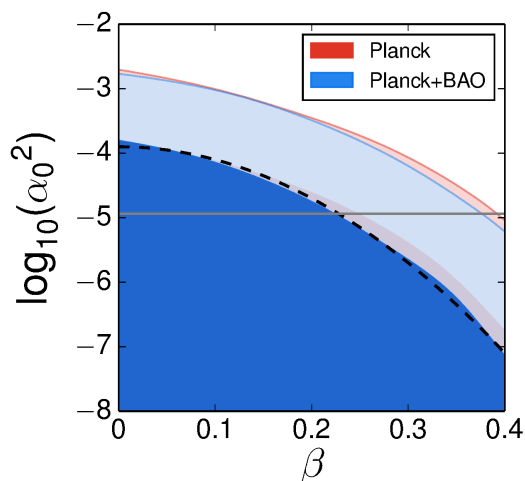


Fig. 6 95.45% and 99.99% confidence contours in the $\log_{10}(\alpha_0^2) - \beta$ plane for the scalar-tensor Λ CDM models with the other parameters marginalized, using the Planck data only (red) or the Planck+BAO data (blue). The black dashed line shows the function $\log_{10}(\alpha_0^2) = -3.9 - 20\beta^2$ and the gray solid line shows the bound from the Solar System experiment.

Table 1 shows 68.27% confidence limits of the standard cosmological parameters in the scalar-tensor Λ CDM model. These parameters are still consistent with those of the Planck results [9] in the standard Λ CDM model. Table 2 shows 95.45% confidence limits of the parameters $\log_{10}(\alpha_0^2)$ and β .

Next, we consider the variation of the gravitational constant in the recombination epoch. We define $G_{\text{rec}} \equiv G(\phi_{\text{rec}})$ and put constraints on G_{rec}/G_0 , after marginalizing over the other parameters. Here, ϕ_{rec} is the value of ϕ at the recombination epoch when the visibility function takes its maximum value. We compute the marginalized posterior distribution of G_{rec}/G_0 as shown in Fig. 7 (for flat models). We find that G_{rec}/G_0 is constrained as

$$G_{\text{rec}}/G_0 - 1 < 1.9 \times 10^{-3} \quad (95.45\%), \quad (19)$$

$$G_{\text{rec}}/G_0 - 1 < 5.5 \times 10^{-3} \quad (99.99\%). \quad (20)$$

These are 10% improvements over the results obtained by the Planck data alone: $G_{\text{rec}}/G_0 - 1 < 2.1 \times 10^{-3}$ (6.0×10^{-3}) at 95.45% C.L. (99.99% C.L.).

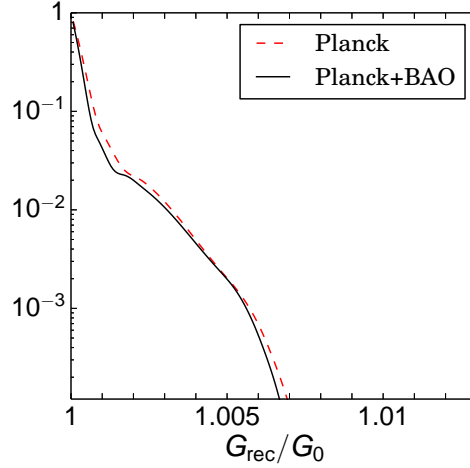


Fig. 7 Posterior distribution of G_{rec}/G_0 , using the Planck data only (red dashed) or the Planck+BAO data (black).

Table 1 68.27% confidence limits for the standard cosmological parameters in the scalar-tensor Λ CDM model.

Parameter	68.27% limits		
	$\Omega_K = 0$	$\Omega_K \neq 0$	$N_{\text{eff}} \neq \text{const.}$
$\Omega_b h^2$	0.02232 ± 0.00014	0.02225 ± 0.00015	0.02231 ± 0.00019
$\Omega_c h^2$	0.1183 ± 0.0011	0.1193 ± 0.0014	0.1182 ± 0.0028
H_0	68.00 ± 0.49	68.53 ± 0.74	67.96 ± 1.17
τ_{reio}	0.072 ± 0.012	0.069 ± 0.012	0.072 ± 0.012
$\ln(10^{10} A_s)$	3.074 ± 0.023	3.071 ± 0.023	3.075 ± 0.024
n_s	0.9675 ± 0.0042	0.9651 ± 0.0049	0.9672 ± 0.0071
Ω_K	—	0.0019 ± 0.0020	—
N_{eff}	—	—	3.035 ± 0.170

Table 2 95.45% confidence limits for $\log_{10}(\alpha_0^2)$ and β .

Parameter	95.45% limits		
	$\Omega_K = 0$	$\Omega_K \neq 0$	$N_{\text{eff}} \neq \text{const.}$
$\log_{10}(\alpha_0^2)$	< -4.56	< -4.58	< -4.48
β	< 0.418	< 0.423	< 0.417

4.2. Nonflat universe case

We also perform a MCMC analysis including spatial curvature parameter Ω_K . This is motivated by the fact that the attractor model used in this paper would predict larger gravitational constant in the past, pushing the acoustic peaks toward smaller angular scales. This effect could be compensated with the positive curvature which brings back the peaks toward larger angles (Nagata *et al.* [7]). This degeneracy, however, should be broken using the CMB data on diffusion damping scales, because the curvature does not affect the diffusion damping whereas the variation of the gravitational constant does as discussed above.

The constraints on the parameters $\log_{10}(\alpha_0^2)$ and β in nonflat models are shown in Fig. 8, where the other parameters including Ω_K are marginalized. We find that the constraints on the scalar-tensor coupling parameters are hardly affected by the inclusion of the spatial curvature. This is because the angular power spectrum on small angular scales obtained from Planck is so precise as to break the degeneracy between the effects of varying gravitational constant and the spatial curvature. We find that $\log_{10}(\alpha_0^2)$ is constrained approximately as

$$\log_{10}(\alpha_0^2) < -3.9 - 18\beta^2 \quad (95.45\%), \quad (21)$$

$$\log_{10}(\alpha_0^2) < -2.7 - 18\beta^2 \quad (99.99\%), \quad (22)$$

and the coupling parameter ω as

$$\omega > 3124 \quad (95.45\%), \quad (23)$$

$$\omega > 258 \quad (99.99\%). \quad (24)$$

We find that the inclusion of the spatial curvature does not much affect the constraint at 95.45% confidence limit, while slightly weakens the constraint at 99.99% confidence limit.

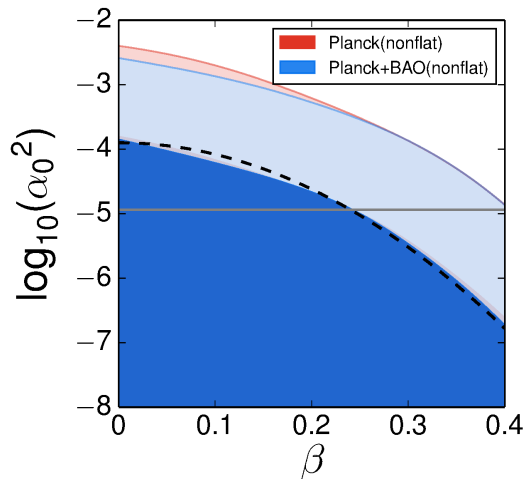


Fig. 8 95.45% and 99.99% confidence contours in the $\log_{10}(\alpha_0^2) - \beta$ plane for the scalar-tensor nonflat Λ CDM models with the other parameters marginalized for the Planck data only (red) or for the Planck+BAO data (blue). The black dashed line and the gray solid line show the function $\log_{10}(\alpha_0^2) = -3.9 - 18\beta^2$ and the bound from the Solar System experiment, respectively.

Also we find that G_{rec}/G_0 in the nonflat universe is constrained as

$$G_{\text{rec}}/G_0 - 1 < 1.9 \times 10^{-3} \quad (95.45\%), \quad (25)$$

$$G_{\text{rec}}/G_0 - 1 < 6.2 \times 10^{-3} \quad (99.99\%). \quad (26)$$

The posterior distribution of G_{rec}/G_0 is shown in Fig. 9. The inclusion of the spatial curvature makes only minor changes on the constraints. The center column in Table 1 shows 68.27% confidence limits of the cosmological parameters in the scalar-tensor nonflat Λ CDM model. These parameters are also still consistent with the those of the Planck results [9]. The limits on the $\log_{10}(\alpha_0^2)$ and β are summarized in Table 2.

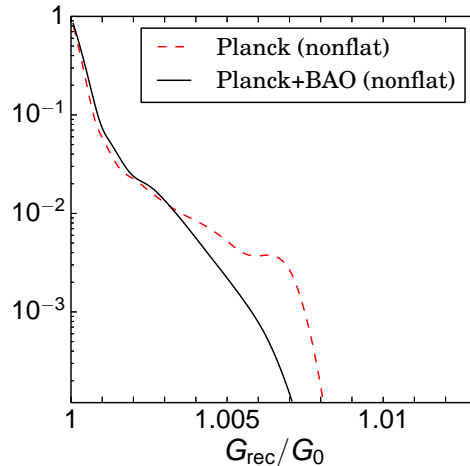


Fig. 9 Posterior distribution of G_{rec}/G_0 for the nonflat models, using the Planck data only (red dashed) or the Planck+BAO data (black).

4.3. Flat universe case including N_{eff}

Additionally, we perform a MCMC analysis including the effective number of relativistic degree of freedom N_{eff} . This is motivated by the fact that the attractor model used in this paper would predict larger Hubble parameter value in the past. This effect could be compensated with the smaller N_{eff} , which predicts the smaller Hubble parameter particularly before the recombination epoch and alter the diffusion damping scale. This degeneracy, however, should be broken if we consider the distance to the CMB, because the energy density of radiation components decays away in the matter dominated era while the variation of the gravitational constant continues to affect the expansion of the universe during that era. The constraints on the parameters $\log_{10}(\alpha_0^2)$ and β in models with N_{eff} are shown in Fig. 10, where the other parameters including N_{eff} are marginalized. We find that the constraints on the scalar-tensor coupling parameters are slightly affected by the inclusion of N_{eff} . We find that $\log_{10}(\alpha_0^2)$ is constrained approximately as

$$\log_{10}(\alpha_0^2) < -3.8 - 20\beta^2 \quad (95.45\%), \quad (27)$$

$$\log_{10}(\alpha_0^2) < -2.6 - 20\beta^2 \quad (99.99\%), \quad (28)$$

and the coupling parameter ω as

$$\omega > 2917 \quad (95.45\%), \quad (29)$$

$$\omega > 177 \quad (99.99\%). \quad (30)$$

We find that the inclusion of N_{eff} slightly weakens the constraints.

Also we find that G_{rec}/G_0 in the case including N_{eff} is constrained as

$$G_{\text{rec}}/G_0 - 1 < 2.5 \times 10^{-3} \quad (95.45\%), \quad (31)$$

$$G_{\text{rec}}/G_0 - 1 < 6.8 \times 10^{-3} \quad (99.99\%). \quad (32)$$

The right column in Table 1 shows 68.27% confidence limits of the cosmological parameters in the scalar-tensor Λ CDM model including N_{eff} . These parameters are also still consistent with the those of the Planck results [9]. The limits on the $\log_{10}(\alpha_0^2)$ and β are summarized in Table 2.

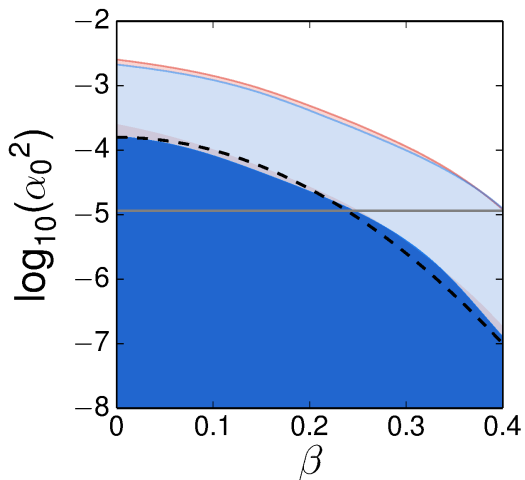


Fig. 10 95.45% and 99.99% confidence contours in the $\log_{10}(\alpha_0^2) - \beta$ plane for the scalar-tensor flat Λ CDM models including N_{eff} with the other parameters marginalized for the Planck data only (red) or for the Planck+BAO data (blue). The black dashed line and the gray solid line show the function $\log_{10}(\alpha_0^2) = -3.8 - 20\beta^2$ and the bound from the Solar System experiment, respectively.

4.4. Choice of Prior

So far, we have performed the analysis using the flat prior on $\log \alpha_0$. In fact, it is equally possible to perform the analysis using the flat prior on α_0 . There seems no preference for the choice of the prior. However, the distributions of the prior differ greatly depending on the choice of variable: from the Jacobian due to the change of variable in the distribution function, the uniform distribution in terms of α_0 , $P(\alpha_0) = \text{const.}$, corresponds to a preference for large $\log \alpha_0$ in terms of $\log \alpha_0$, $P(\log \alpha_0) \propto \exp(\log \alpha_0)$, or the uniform $P(\log \alpha_0)$ corresponds to a preference for small α_0 in terms of α_0 , $P(\alpha_0) \propto 1/\alpha_0$. In this section, we discuss the consequence of the choice of the prior for the constraints on the parameters. The effects of the choices of priors in the anisotropic universes are discussed in [20].

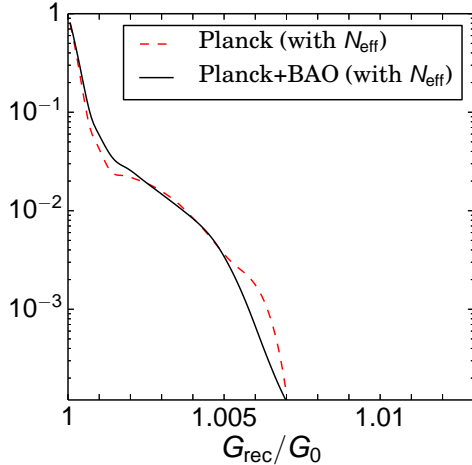


Fig. 11 Posterior distribution of G_{rec}/G_0 for the flat models with N_{eff} , using the Planck data only (red dashed) or the Planck+BAO data (black).

We perform the analysis using the uniform prior on α_0 . Namely, instead of Eq. 9, we set

$$\alpha_0 \in (0, 0.5). \quad (33)$$

The priors on the other parameters are the same as Eq. (8) and Eq. (10).

In Fig. 12, the constraints in the $\alpha_0^2 - \beta$ plane are shown for both the linear prior and logarithmic prior cases. The posterior distribution functions for G_{rec}/G_0 are shown in Fig. 13.

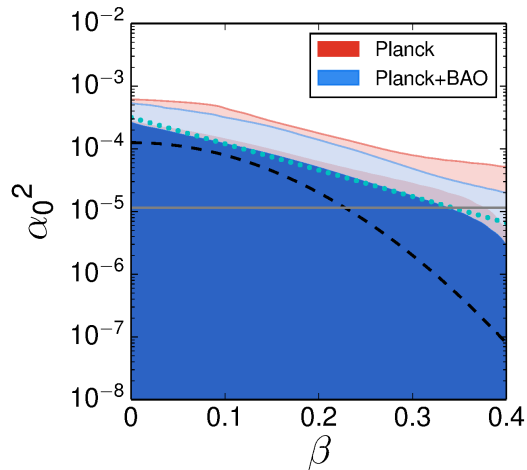


Fig. 12 95.45% and 99.99% confidence contours in the $\alpha_0^2 - \beta$ plane for the scalar-tensor Λ CDM models with the other parameters marginalized, using the Planck+BAO data. The cyan dotted line show the function $\alpha_0^2 = 10^{-3.5-4.2\beta}$. The black dashed line and the gray solid line are the same as Fig. 6.

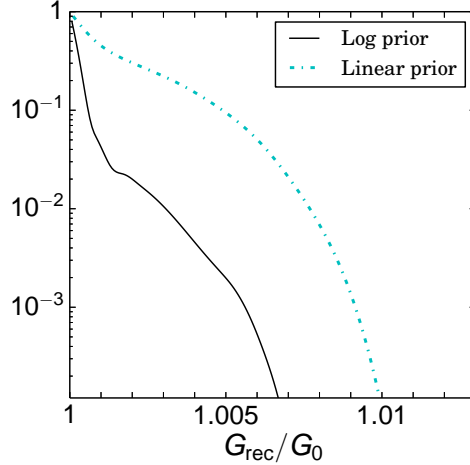


Fig. 13 Posterior distribution of G_{rec}/G_0 .

With the linear prior, we find that α_0^2 is constrained as

$$\log_{10}(\alpha_0^2) < -3.5 - 4.2\beta \quad (95.45\%), \quad (34)$$

$$\log_{10}(\alpha_0^2) < -3.2 - 4.2\beta \quad (99.99\%), \quad (35)$$

and the coupling parameter ω as

$$\omega > 2009 \quad (95.45\%), \quad (36)$$

$$\omega > 907 \quad (99.99\%). \quad (37)$$

95.45% confidence limit of ω is almost the same as our previous results in [10], while the constraint at 99.99% confidence limit is strengthened.

G_{rec}/G_0 is constrained as

$$G_{\text{rec}}/G_0 - 1 < 5.2 \times 10^{-3} \quad (95.45\%), \quad (38)$$

$$G_{\text{rec}}/G_0 - 1 < 8.9 \times 10^{-3} \quad (99.99\%). \quad (39)$$

These are 7% (95.45%) or 20% (99.99%) improvement over our previous results obtained by the Planck data alone: $G_{\text{rec}}/G_0 - 1 < 5.6 \times 10^{-3}$ (11.5×10^{-3}) at 95.45% C.L. (99.99% C.L.) [10]. Therefore, the statistical merit of including BAO is more significant in the linear-prior case than in the log-prior case. We find that the constraint on $\alpha_0^2 - \beta$ and the constraint on G with the linear prior are more relaxed than those with the flat prior on $\log_{10}(\alpha_0)$.

5. Summary

We have constrained the scalar-tensor Λ CDM model from the Planck data and the BAO data by using the MCMC method. We have found that the present-day deviation from the Einstein gravity (α_0^2) is constrained as $\log_{10}(\alpha_0^2) < -3.9 - 20\beta^2$ (95.45% C.L.) and $\log_{10}(\alpha_0^2) < -2.8 - 20\beta^2$ (99.99% C.L.) for $0 < \beta < 0.4$. The variation of the gravitational constant is also constrained as $G_{\text{rec}}/G_0 < 1.0019$ (95.45% C.L.) and $G_{\text{rec}}/G_0 < 1.0055$ (99.99% C.L.). These constraints are improved more than 10% compared with the results obtained by

the Planck data alone. We have also found that these constraints are not much affected by the inclusion of the spatial curvature or the effective number of relativistic degree of freedom N_{eff} . We have discussed the prior dependence of the analysis and found that the constraints using the flat prior on α_0 are slightly relaxed: $G_{\text{rec}}/G_0 < 1.0052$ (95.45% C.L.) and $G_{\text{rec}}/G_0 < 1.0089$ (99.99% C.L.).

Acknowledgment

This work is in part supported by MEXT Grant-in-Aid for Scientific Research on Innovative Areas, Nos. 15H05890 (NS and KI) and 15H05894 (TC). This work is also supported by the Grant-in-Aid for Scientific Research from JSPS (Nos. 24540287 (TC), 24340048 (KI) and 25287057 (NS)), and in part by Nihon University (TC).

A. Einstein frame and the Harmonic Attractor Model

In this appendix, we explain the details about the choice of Eq. (2). We define the Einstein frame metric $\bar{g}_{\mu\nu}$ by the conformal transformation of the form

$$g_{\mu\nu} = \frac{1}{\phi} \bar{g}_{\mu\nu} \equiv e^{2a} \bar{g}_{\mu\nu}. \quad (\text{A1})$$

Then, Eq. (1) can be rewritten as

$$S = \frac{1}{16\pi G_0} \int d^4x \sqrt{-\bar{g}} \left[\bar{R} - \left(\omega(\phi) + \frac{3}{2} \right) \frac{(\bar{\nabla}\phi)^2}{\phi^2} \right] + S_{\text{m}}[\psi, e^{2a} \bar{g}_{\mu\nu}]. \quad (\text{A2})$$

We introduce the normalized scalar field φ by

$$\left(\omega(\phi) + \frac{3}{2} \right) \frac{(d\phi)^2}{\phi^2} = 2(d\varphi)^2. \quad (\text{A3})$$

From Eq. (A1), $\omega(\phi)$ is related to $a(\varphi)$ by

$$2\omega + 3 = \left(\frac{da}{d\varphi} \right)^{-2}. \quad (\text{A4})$$

Note that the extrema of $a(\varphi)$ corresponds to $\omega \rightarrow \infty$ (the Einstein gravity). Since the cosmological evolution of φ is determined $\ddot{\varphi} + 3\bar{H}\dot{\varphi} = -4\pi G_0 (da/d\varphi)(\bar{\rho} - 3\bar{p})$ (where barred quantities are to be regarded as those in the Einstein frame) [8], we can regard that $a(\varphi)$ is (proportional to) the effective potential. We Taylor-expand $a(\varphi)$ around the present time up to the quadratic order:

$$a(\varphi) = a_0 + \alpha_0(\varphi - \varphi_0) + \frac{1}{2}\beta(\varphi - \varphi_0)^2. \quad (\text{A5})$$

From Eq. (A4), in terms of $\phi = e^{-2a}$, this generic choice of $a(\varphi)$ corresponds to Eq. (2).

References

- [1] M.B. Green, J.H. Schwarz and E. Witten, *Superstring theory:1* (Cambridge University Press, Cambridge, UK, 1987).
- [2] P. Jordan, *Z. Phys.* **157**, 112 (1959); C. Brans and R. H. Dicke, *Phys. Rev.* **124**, 925 (1961).
- [3] P. G. Bergmann, *Int. J. Theor. Phys.* **1**, 25 (1968); K. Nordtvedt, Jr., *Astrophys. J.* **161**, 1059 (1970); R. V. Wagoner, *Phys. Rev. D* **1**, 3209 (1970).
- [4] B. Bertotti, L. Iess and P. Tortora, *Nature* **425**, 374 (2003).

-
- [5] C. M. Will, *Living Rev. Rel.* **17**, 4 (2014) [arXiv:1403.7377 [gr-qc]].
 - [6] X. I. Chen and M. Kamionkowski, *Phys. Rev. D* **60**, 104036 (1999) [astro-ph/9905368].
 - [7] R. Nagata, T. Chiba and N. Sugiyama, *Phys. Rev. D* **69**, 083512 (2004) [astro-ph/0311274].
 - [8] T. Damour and K. Nordtvedt, *Phys. Rev. Lett.* **70**, 2217 (1993); T. Damour and K. Nordtvedt, *Phys. Rev. D* **48**, 3436 (1993).
 - [9] P. A. R. Ade *et al.* [Planck Collaboration], arXiv:1502.01589 [astro-ph.CO].
 - [10] J. Ooba, K. Ichiki, T. Chiba and N. Sugiyama, *Phys. Rev. D* **93**, no. 12, 122002 (2016) doi:10.1103/PhysRevD.93.122002 [arXiv:1602.00809 [astro-ph.CO]].
 - [11] F. Beutler, C. Blake, M. Colless, D. H. Jones, L. Staveley-Smith, L. Campbell, Q. Parker, W. Saunders, F. Watson *Mon. Not. Roy. Astron. Soc.* **416**, 3017, (2011)
 - [12] L. Anderson *et al.* [BOSS Collaboration], *Mon. Not. Roy. Astron. Soc.* **441**, no. 1, 24 (2014).
 - [13] A. J. Ross, L. Samushia, C. Howlett, W. J. Percival, A. Burden and M. Manera, *Mon. Not. Roy. Astron. Soc.* **449**, no. 1, 835 (2015).
 - [14] R. Nagata, T. Chiba and N. Sugiyama, *Phys. Rev. D* **66**, 103510 (2002) [astro-ph/0209140].
 - [15] T. Damour and G. Esposito-Farese, *Class. Quant. Grav.* **9**, 2093 (1992).
 - [16] T. Chiba and M. Yamaguchi, *J. Cosmo. Astropart. Phys.* 10 (2013) 040, [arXiv:1308.1142 [gr-qc]].
 - [17] D. Blas, J. Lesgourgues and T. Tram, *J. Cosmo. Astropart. Phys.* 07 (2011) 034.
 - [18] B. Audren, J. Lesgourgues, K. Benabed and S. Prunet, *J. Cosmo. Astropart. Phys.* 02 (2013) 001.
 - [19] D. J. Fixsen, *Astrophys. J.* **707**, 916 (2009).
 - [20] D. Saadeh, S. M. Feeney, A. Pontzen, H. V. Peiris and J. D. McEwen, arXiv:1604.01024 [astro-ph.CO].